Hindawi Publishing Corporation
Advances in Tribology
Volume 2012, Article ID 898252, 18 pages
doi:10.1155/2012/898252

Research Article

Influence of Micropolar Lubrication on the Performance of 4-Pocket Capillary Compensated Conical Hybrid Journal Bearing

Satish C. Sharma and Arvind K. Rajput

Tribology Laboratory, Department of Mechanical and Industrial Engineering, Indian Institute of Technology Roorkee, Roorkee 247667, India

Correspondence should be addressed to Arvind K. Rajput, arvind.mechei@gmail.com

Received 15 May 2012; Revised 18 July 2012; Accepted 20 August 2012

Academic Editor: Patrick De Baets

The present paper deals with a theoretical analysis of 4-pocket capillary compensated conical hybrid journal bearing system operating with micropolar lubricant. The modified Reynolds equation for a conical journal bearing system operating with micropolar lubricant has been derived. In the present study, Eringen's micropolar theory has been used to model micropolar lubrication in cylindrical coordinate system. The study has been carried out for the different values of micropolar parameters, that is, characteristic length ($\bar{l}$) and coupling number (N). The conical bearing configurations having semicone angle 10°, 20°, 30°, and 40° have been studied. The study suggests that micropolar lubricant offers better performance vis- á-vis Newtonian lubricant for bearing configurations having values of semicone angle 10° and 20°.

1. Introduction

The noncircular journal bearings such as lobed bearing, pressure dam bearing, and conical journal bearing provide better performance than that of the circular journal bearings for different considerations. Conical journal bearing system can support both radial and axial load within less space vis-á-vis different combinations of circular journal and rotary thrust bearing. These bearings are also more economical for the machining point of view [1, 2]. In recent times, many researchers have focused their studies [2–15] concerning the analysis and design of conical bearings.

Murthy et al. [3] studied a new type of conical multilobe special precision bearing. It was reported that axial preload and lobe depth affect the working clearance and the fluid film stiffness of the bearing significantly. Prabhu and Ganesan [4, 6, 7] analyzed the dynamic stiffness characteristics of capillary compensated annular recess conical hydrostatic thrust bearings. In their study, they discussed the conditions of tilt, eccentricity, and rotation. Srinivasan and Prabhu [5] studied the steady state performance of externally pressurized gas-lubricant conical bearings under rotation. The influence of bearing operating parameters on the radial and axial load capacity, attitude angle, friction loss, and stiffness was discussed for the semicone angle 10°–40°. Khalil et al. [8] investigated the influence of turbulent lubrication on the performance of an externally pressurized circular and conical thrust bearings. Both the inertia forces and thermal effects were neglected. Their study indicates that the circular thrust bearing has slightly higher dimensionless pressure, load, and torque than the conical thrust bearing.

The mono and multigrade lubricants used in present day industrial applications are blended with additives which are polymeric in nature. This blending results into deviation of lubricant rheology from Newtonian to non-Newtonian (nonlinear). Yousif and Nacy [9] presented experimental and theoretical studies dealing with the effect of solid additives in lubricating oils on the steady state performance of conical journal bearings using the mass transfer theory. Yoshimoto et al. [10, 11] investigated water-lubricated hydrostatic conical bearings with spiral grooves for high-speed spindles. It was found that the compliant surface bearing had a larger load capacity in a relatively large bearing clearance than the rigid surface bearing and lower bearing

power consumption in a small bearing clearance although the load capacity is reduced. Abdel-Rahman [12] used an average clearance method to solve the equation of stationary pressure distribution in flow between the conical surfaces. Li et al. [13] studied Taylor vortex flow between two conical cylinders, with the inner one rotating and the outer one stationary by the numerical method. It was found that the basic flow becomes unstable with an increase in Reynolds number (Re) above a certain critical value (Re = 117) and with the further increase of Re (to about Re = 300), the first stable vortex is formed near the top of the flow system. These were confirmed by experimental observations. Sharma et al. [14, 15] carried out a theoretical study of a 4-pocket hydrostatic conical journal bearing system. The bearing static and dynamic performance characteristics were presented for the values of external load ranging $\overline{W}_r$ = 0.1–1.0 and for the values of semicone angles (γ = 10°, 20°, 30°, and 40°). The influence of wear in the analysis of a four- pocket orifice compensated hybrid conical journal bearing was considered [15]. The studies [14, 15] were limited for Newtonian lubricants only. Very recently Zhang et al. [16] studied the end plate effect on Taylor vortices between rotating conical cylinders. It was reported that the number of vortices increases with decreasing of the gap size and the end plates play an important role in the parity of the number of the vortices.

The lubricant plays a vital role on the overall performance of bearing. A lot of research has been carried out with non Newtonian lubricants. Polymer additives are mixed to the Newtonian lubricant in order to improve their performance characteristics. These polymer additives have the different flow characteristics than the parent fluid. There are many theories available to describe the flow characteristics of non-Newtonian lubricants such as electrorheological lubricant, coupled stress lubricant, and micropolar lubricant. The theory of micropolar fluid gives the best descriptions of the non-Newtonian fluids containing additives substructures. There are many physical examples of micropolar fluids as ferrofluids, blood flows, bubbly liquids, liquid crystals [17]. This class of fluids exhibit special properties to support couple stress and body couple due to their microstructure and microrotational inertia at microscopic level. The theory of micropolar fluids was formulated by Eringen [18]. The first application of micropolar lubricant in fluid film bearings was carried out by Allen and Kline [19]. Prakash and Sinha [20] discussed the lubrication theory for micropolar fluid. They assumed a two dimensional flow field and gave argument for order of magnitude analysis. Later on, Singh and Sinha [21] derived 3-dimensional Reynolds equation for micropolar lubricated cylindrical journal bearing. Huang et al. [22] and Khonsari and Brewe [23] obtained steady state characteristics of finite-width journal bearings with micropolar lubricants. Huang and Weng [24] presented the study of the dynamic characteristics of finite-width journal bearings with micropolar lubricants. They observed that it is easier for the oil whirl to occur in a micropolar fluid under low Sommerfield number condition, although the micropolar fluid increases the effective viscosity and load capacity. Wang and Zhu [25] studied the lubricating effectiveness of micropolar lubricants in a dynamically loaded journal bearing. Das et al. [26] presented the dynamic characteristics of hydrodynamic journal bearings lubricated with micropolar lubricants. Their results showed that micropolar fluid exhibits better stability in comparison with Newtonian fluid. A numerical study of the non-Newtonian behavior for a finite journal bearing lubricated with micropolar fluids was carried out by Wang and Zhu [27]. They studied the influence of material characteristic length and the coupling number on the thermohydrodynamic performance of a journal bearing.

Nair et al. [28] considered the effect of deformation of the bearing liner on the static and dynamic performance characteristics of an elliptical journal bearing operating with micropolar lubricant. Rahmatabadi et al. [29] considered the noncircular bearing configurations for two-, three- and four-lobe bearings lubricated with micropolar lubricants.

A thorough scan of the existing literature reveals that the available studies in the area of conical hydrostatic and hybrid journal bearing system have been mainly restricted to Newtonian lubricant. Now a days the lubricants are additized in order to improve their lubricating performance. As a consequence of which, they exhibit nonlinear behavior and the analysis becomes quite involved. Therefore, the present work is planned to bridge the gap in literature and to analyze the conical hybrid journal bearing system operating with micropolar lubricant as shown in Figure 1(a). The numerically simulated results in present study are expected to be beneficial to bearing designers as well as to academic community.

2. Analysis

The governing equations describing the behavior of micropolar lubricants as derived by Eringen [18] are expressed as

$$\begin{aligned}
&\frac{\partial \rho}{\partial t} + \nabla(\rho.V) = 0,\\
&(\lambda' + 2\mu)\nabla(\nabla \cdot V) - \frac{1}{2}\left(2\mu + \chi\right)\nabla \times \nabla\\
&\qquad \times V + \chi\nabla \times \vartheta - \nabla p + \rho B = \rho\frac{DV}{Dt},\\
&(\alpha_1 + \beta_1 + \gamma_1)\nabla(\nabla \cdot \vartheta) - \gamma_1\nabla \times \nabla\\
&\qquad \times \vartheta + \chi\nabla \times V - 2\chi\vartheta + \rho L' = \rho J\frac{D\vartheta}{Dt}.
\end{aligned} \tag{1}$$

In a conical journal bearing system, clearance between the journal and bearing is very small and the ratio of the fluid film thickness to the mean radius of conical journal approaches to 10^{-3} to 10^{-4}. Therefore a conical journal bearing system can be modeled as flow of lubricant between two curvilinear plates as shown in Figure 1(b). Thus in cylindrical coordinate (θ, R, z) system, the velocity,

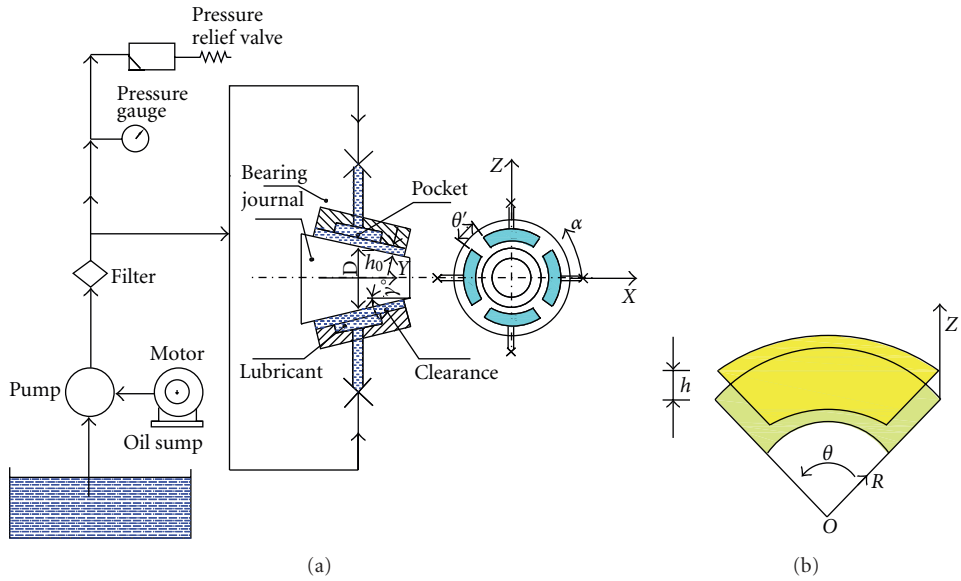

Figure 1: (a) Schematic of conical journal bearing system. (b) Developed surfaces of conical journal bearing system in cylindrical coordinates.

microrotation velocity, and pressure for a conical hybrid journal bearing system may be expressed as

$$\begin{aligned} V &= (V_1(R,\theta,z), V_2(R,\theta,z), V_3(R,\theta,z)),\\ \vartheta &= (\vartheta_1(R,\theta,z), \vartheta_2(R,\theta,z), \vartheta_3(R,\theta,z)),\\ p &= p(R,\theta,z). \end{aligned} \tag{2}$$

In cylindrical coordinate system, for a steady incompressible flow ($\nabla \cdot V = 0$), (1) can be written as follows:

$$\frac{1}{R}\frac{\partial(RV_1)}{\partial R} + \frac{1}{R}\frac{\partial V_2}{\partial \theta} + \frac{\partial V_3}{\partial z} = 0, \tag{3}$$

$$\begin{aligned} &\frac{1}{2}(2\mu+\chi)\left[\frac{\partial^2}{\partial R^2} + \frac{1}{R}\frac{\partial}{\partial R} + \frac{1}{R^2}\frac{\partial^2}{\partial \theta^2} + \frac{\partial^2}{\partial z^2}\right]V_1\\ &+\chi\left[\frac{1}{R}\frac{\partial \vartheta_3}{\partial \theta} - \frac{\partial \vartheta_2}{\partial z}\right] - \frac{\partial p}{\partial R} + \rho B_R\\ &= \rho\left[V_1\frac{\partial V_1}{\partial R} + \frac{V_2}{R}\frac{\partial V_1}{\partial \theta} + V_3\frac{\partial V_1}{\partial z} - \frac{{V_1}^2}{R}\right], \end{aligned} \tag{4}$$

$$\begin{aligned} &\frac{1}{2}(2\mu+\chi)\left[\frac{\partial^2}{\partial R^2} + \frac{1}{R}\frac{\partial}{\partial R} + \frac{1}{R^2}\frac{\partial^2}{\partial \theta^2} + \frac{\partial^2}{\partial z^2}\right]V_2\\ &+\chi\left[\frac{\partial \vartheta_1}{\partial z} - \frac{\partial \vartheta_3}{\partial R}\right] - \frac{1}{R}\frac{\partial p}{\partial \theta} + \rho B_\theta\\ &= \rho\left[V_1\frac{\partial V_2}{\partial R} + \frac{V_2}{R}\frac{\partial V_2}{\partial \theta} + V_3\frac{\partial V_2}{\partial z} + \frac{V_1 V_2}{R}\right], \end{aligned} \tag{5}$$

$$\begin{aligned} &\frac{1}{2}(2\mu+\chi)\left[\frac{\partial^2}{\partial R^2} + \frac{1}{R}\frac{\partial}{\partial R} + \frac{1}{R^2}\frac{\partial^2}{\partial \theta^2} + \frac{\partial^2}{\partial z^2}\right]V_3\\ &+\chi\left[\frac{\partial \vartheta_2}{\partial R} - \frac{1}{R}\frac{\partial \vartheta_1}{\partial \theta}\right] - \frac{\partial p}{\partial z} + \rho B_Z\\ &= \rho\left[V_1\frac{\partial V_3}{\partial R} + \frac{V_2}{R}\frac{\partial V_3}{\partial \theta} + V_3\frac{\partial V_3}{\partial z}\right], \end{aligned} \tag{6}$$

$$\begin{aligned} &\gamma_1\left[\frac{\partial^2}{\partial R^2} + \frac{1}{R}\frac{\partial}{\partial R} + \frac{1}{R^2}\frac{\partial^2}{\partial \theta^2} + \frac{\partial^2}{\partial z^2}\right]\vartheta_1\\ &+\chi\left[\frac{1}{R}\frac{\partial V_3}{\partial \theta} - \frac{\partial V_2}{\partial z}\right] - 2\chi\vartheta_1 + \rho L'_R\\ &= \rho J\left[\vartheta_1\frac{\partial \vartheta_1}{\partial R} + \frac{\vartheta_2}{R}\frac{\partial \vartheta_1}{\partial \theta} + \vartheta_3\frac{\partial \vartheta_1}{\partial z} - \frac{{\vartheta_1}^2}{R}\right], \end{aligned} \tag{7}$$

$$\begin{aligned} &\gamma_1\left[\frac{\partial^2}{\partial R^2} + \frac{1}{R}\frac{\partial}{\partial R} + \frac{1}{R^2}\frac{\partial^2}{\partial \theta^2} + \frac{\partial^2}{\partial z^2}\right]\vartheta_2\\ &+\chi\left[\frac{\partial V_1}{\partial z} - \frac{\partial V_3}{\partial R}\right] - 2\chi\vartheta_2 + \rho L'_\theta\\ &= \rho J\left[\vartheta_1\frac{\partial \vartheta_2}{\partial R} + \frac{\vartheta_2}{R}\frac{\partial \vartheta_2}{\partial \theta} + \vartheta_3\frac{\partial \vartheta_2}{\partial z} + \frac{\vartheta_1\vartheta_2}{R}\right], \end{aligned} \tag{8}$$

$$\begin{aligned} &\gamma_1\left[\frac{\partial^2}{\partial R^2} + \frac{1}{R}\frac{\partial}{\partial R} + \frac{1}{R^2}\frac{\partial^2}{\partial \theta^2} + \frac{\partial^2}{\partial z^2}\right]\vartheta_3\\ &+\chi\left[\frac{\partial V_2}{\partial R} - \frac{1}{R}\frac{\partial V_1}{\partial \theta}\right] - 2\chi\vartheta_3 + \rho L'_z\\ &= \rho J\left[\vartheta_1\frac{\partial \vartheta_3}{\partial R} + \frac{\vartheta_2}{R}\frac{\partial \vartheta_3}{\partial \theta} + \vartheta_3\frac{\partial \vartheta_3}{\partial z}\right]. \end{aligned} \tag{9}$$

2.1. Assumptions. In general, the following assumptions are made in the analysis of a journal bearing system using micropolar theory.

(i) Body force and body couples are negligible.

(ii) The inertia forces and inertia couples are very small, and therefore neglected.

(iii) All the characteristics coefficients are independent of z.

(iv) For steady incompressible fluids, $\nabla \cdot V = 0$.

(v) The pressure variation in Z direction is negligible.

(vi) Flow of lubricant in the clearance space between the journal and bearing is two dimensional.

(vii) The velocity and microrotation velocity fields are independent of R direction.

The velocity, microrotation velocity, and pressure, for the conical journal bearing system as shown in Figure 1 are given as follows:

$$\begin{aligned} V &= (V_1(\theta,z), V_2(\theta,z), 0), \\ \vartheta &= (\vartheta_1(\theta,z), \vartheta_2(\theta,z), 0), \\ p &= p(\theta,R). \end{aligned} \tag{10}$$

Incorporating the above assumptions and order of the magnitude analysis, ((4)–(9)) reduces to the following forms:

$$\begin{aligned} \frac{1}{2}\left(2\mu+\chi\right)\frac{\partial^2 V_1}{\partial z^2} - \chi\frac{\partial \vartheta_2}{\partial z} - \frac{\partial p}{\partial R} &= 0, \\ \frac{1}{2}\left(2\mu+\chi\right)\frac{\partial^2 V_2}{\partial z^2} + \chi\frac{\partial \vartheta_1}{\partial z} - \frac{1}{R}\frac{\partial p}{\partial \theta} &= 0, \\ \gamma_1\frac{\partial^2 \vartheta_1}{\partial z^2} - 2\chi\vartheta_1 - \chi\frac{\partial V_2}{\partial z} &= 0, \\ \gamma_1\frac{\partial^2 \vartheta_2}{\partial z^2} - 2\chi\vartheta_2 + \chi\frac{\partial V_1}{\partial z} &= 0. \end{aligned} \tag{11}$$

To determine the expressions of velocity field for micropolar lubricant, the following boundary conditions are incorporated in (11):

$$\begin{aligned} V_1 = 0, \quad V_2 = U, \quad \vartheta_1 = \vartheta_2 = 0 \quad \text{at } z = 0, \\ V_1 = V_2 = 0, \quad \vartheta_1 = \vartheta_2 = 0 \quad \text{at } z = h. \end{aligned} \tag{12}$$

2.2. The Lubricant Flow. The local lubricant flow per unit width in R and θ direction can be obtained by integrating the respective velocity components across the local fluid film thickness, expressed as

$$\begin{aligned} q_\theta &= \int_0^h V_2 dz, \\ q_\theta &= \frac{Uh}{2} - \frac{\Phi(N,l,h)}{12\mu}\frac{1}{R}\frac{\partial p}{\partial \theta}, \\ \text{Similarly, } q_R &= \int_0^h V_1 dz = -\frac{\Phi(N,l,h)}{12\mu}\frac{\partial p}{\partial R}, \end{aligned} \tag{13}$$

where $\Phi(N,l,h) = h^3 + 12l^2h - 6Nlh^2\text{Coth}(Nh/2l)$ is known as micropolar function. Consider the following:

$$N = \left(\frac{\chi}{2\mu+\chi}\right)^{1/2}, \qquad l = \left(\frac{\gamma_1}{4\mu}\right)^{1/2}, \tag{14}$$

where N is a dimensionless quantity, named as coupling number, and l has the unit of length, named as characteristic length. These N and l are two main characteristics parameters of micropolar lubricant.

2.3. Modified Reynolds Equations. The continuity equation in cylindrical coordinate system for 2-dimensional flow is given as follows [30]:

$$\frac{\partial \rho}{\partial t} + \frac{1}{R}\frac{\partial\left(\rho R V_1\right)}{\partial R} + \frac{1}{R}\frac{\partial(\rho V_2)}{\partial \theta} = 0. \tag{15}$$

Integrating (15) with respect to z across the fluid film thickness, that is, (0 to h), and using (13), yields

$$\frac{\partial h}{\partial t} + \frac{1}{R}\frac{\partial(Rq_R)}{\partial R} + \frac{1}{R}\frac{\partial q_\theta}{\partial \theta} = 0. \tag{16}$$

Substituting the value of q_R and q_θ in (16), we have

$$\begin{aligned} &\frac{1}{R}\frac{\partial}{\partial R}\left[\frac{R\Phi(N,l,h)}{12\mu}\frac{\partial p}{\partial R}\right] + \frac{1}{R^2}\frac{\partial}{\partial \theta}\left[\frac{\Phi(N,l,h)}{12\mu}\frac{\partial p}{\partial \theta}\right] \\ &\quad = \frac{1}{2}\frac{1}{R}\frac{\partial(Uh)}{\partial \theta} + \frac{\partial h}{\partial t}. \end{aligned} \tag{17}$$

Substituting the values of the parameters as $U = r\omega$, [$\theta = \alpha \sin\gamma$, $R = r\sin\gamma$ (see Figure 2(a)), we have

$$\begin{aligned} &\frac{1}{R}\frac{\partial}{\partial R}\left[\frac{R\Phi(N,l,h)}{12\mu}\frac{\partial p}{\partial R}\right] + \frac{1}{(R\sin\gamma)^2}\frac{\partial}{\partial \alpha}\left[\frac{\Phi(N,l,h)}{12\mu}\frac{\partial p}{\partial \alpha}\right] \\ &\quad = \frac{1}{2}\omega\frac{\partial h}{\partial \alpha} + \frac{\partial h}{\partial t}. \end{aligned} \tag{18}$$

Using the following nondimensional parameter in (18), we get

$$\begin{aligned} \beta &= \frac{R\sin\gamma}{r_j}; \qquad \overline{p} = \frac{p}{p_s}; \qquad \overline{l} = \frac{c}{l}; \\ \overline{h} &= \frac{h}{c}; \qquad \overline{t} = \frac{t}{\left[\mu r_j^2/c^2 p_s\right]}; \\ \Omega &= \frac{\omega_j}{\left[c^2 p_s/\mu r_j^2\right]} : \ \overline{\Phi}\left(N,\overline{l},\overline{h}\right) = \frac{\Phi(N,l,h)}{c^3}. \end{aligned} \tag{19}$$

Nondimensionalization of (18) yields

$$\begin{aligned} &\frac{\sin^2\gamma}{\beta}\frac{\partial}{\partial \beta}\left[\frac{\beta\overline{\Phi}\left(N,\overline{l},\overline{h}\right)}{12}\frac{\partial \overline{p}}{\partial \beta}\right] + \frac{1}{\beta^2}\frac{\partial}{\partial \alpha}\left[\frac{\overline{\Phi}\left(N,\overline{l},\overline{h}\right)}{12}\frac{\partial \overline{p}}{\partial \alpha}\right] \\ &\quad = \frac{1}{2}\Omega\frac{\partial \overline{h}}{\partial \alpha} + \frac{\partial \overline{h}}{\partial \overline{t}}, \end{aligned} \tag{20}$$

where $\overline{\Phi}((N,\overline{l},\overline{h})) = \overline{h}^3 + 12(\overline{h}/\overline{l}^2) - 6(N\overline{h}^2/\overline{l})\text{Coth}(N\overline{h}\overline{l}/2)$.

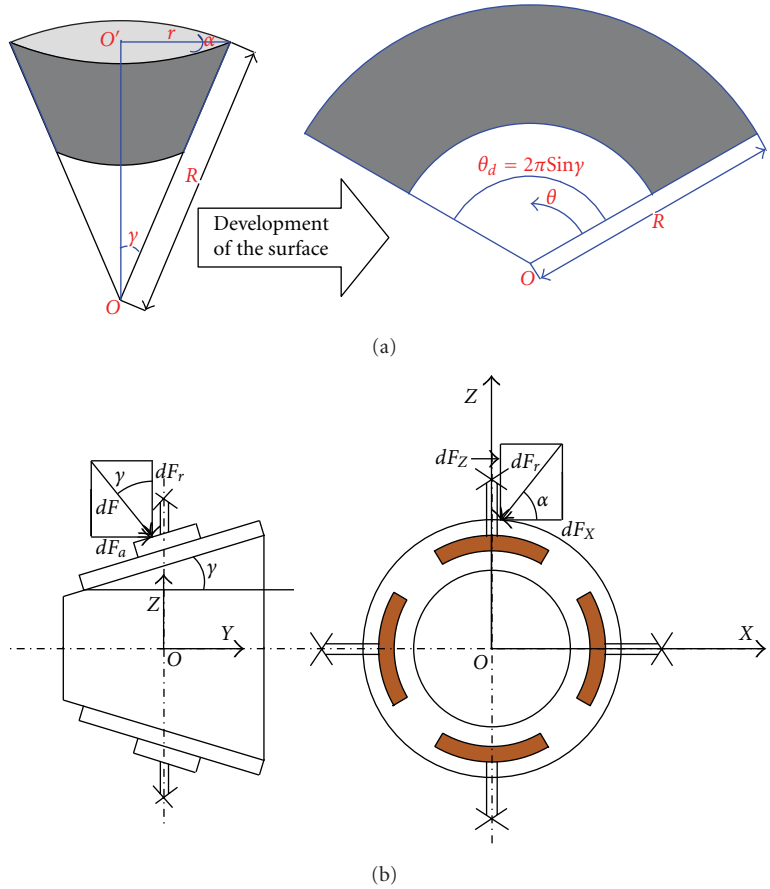

FIGURE 2: (a) Development of the surface of conical journal bearing. (b) Load carrying capacity distribution of a conical journal bearing.

Equation (20) is the modified Reynolds equation for a conical journal bearing system operating with micropolar lubricant. For the values of micropolar parameters, $\bar{l} = \infty$, $N = o$, (20) changes into the form applicable for Newtonian lubricant as given in [14, 15].

2.4. Finite Element Formulation. Applying the finite element method using the orthogonality condition of Galerkin's technique in (20), the following elemental equation (21) in matrix form is obtained:

$$\left[\overline{F}_{ij}\right]^e \{\overline{p}\}^e = \left\{\overline{Q}\right\}^e + \Omega \left\{\overline{R}_H\right\}^e + \overline{X}_j \left\{\overline{R}_{X_j}\right\}^e + \overline{Z}_j \left\{\overline{R}_{Z_j}\right\}^e, \tag{21}$$

where

$$\overline{F}^e_{ij} = \iint_{\Omega^e} \left[\frac{\overline{\Phi}\left(N, \bar{l}, \bar{h}\right)}{12} \left(\frac{1}{\sin\gamma} \frac{\partial N_i}{\partial \alpha} \frac{\partial N_j}{\partial \alpha} + \beta^2 \sin\gamma \frac{\partial N_i}{\partial \beta} \frac{\partial N_j}{\partial \beta} \right) \right] d\alpha\, d\beta, \tag{22}$$

$$\overline{Q}^e_i = \oint_{\Gamma^e} \frac{\overline{\Phi}\left(N, \bar{l}, \bar{h}\right)}{12} \left[\frac{1}{\sin\gamma} \frac{\partial \overline{p}}{\partial \alpha} n_\alpha + \beta^2 \sin\gamma \frac{\partial \overline{p}}{\partial \beta} n_\beta \right] \times N_i\, \overline{p}_j d\Gamma - \frac{\Omega}{2} \oint_{\Gamma^e} N_i \frac{\beta^2}{\sin\gamma} \overline{h} n_\alpha\, d\Gamma,$$

$$\overline{R}^e_{Hi} = \frac{1}{2} \iint_{\Omega^e} \overline{h} \frac{\partial N_i}{\partial \alpha} \frac{\beta^2}{\sin\gamma}\, d\alpha\, d\beta,$$

$$\overline{R}^e_{X_j i} = \iint_{\Omega^e} \cos\alpha \cos\gamma \frac{\beta^2}{\sin\gamma} N_i\, d\alpha\, d\beta,$$

$$\overline{R}^e_{Z_j i} = \iint_{\Omega^e} \sin\alpha \cos\gamma \frac{\beta^2}{\sin\gamma} N_i\, d\alpha\, d\beta, \tag{23}$$

where n_α and n_β are the direction cosines and $i, j = 1, 2, 3, 4$ (number of nodes per element). Ω^e represents the area domain and Γ^e is the boundary domain of the eth element.

The Equation (21) represents the finite element formulation of the bearing system. The Equation (21) has been derived by orthogonalizing the residue (From (20)) using Galerkin's technique. The fluid film domain has been discretized using 4-noded isoparametric 2D element.

The fluid film pressure is approximated over an element as follows:

$$\overline{p} = \sum_{j=1}^{4} N_j \overline{p}_j. \tag{24}$$

2.5. Fluid Film Thickness. For a conical journal bearing system, the fluid film thickness in nondimensional form is expressed as [14]

$$\overline{h} = \left(1 - \overline{X}_j \cos\alpha - \overline{Z}_j \sin\alpha\right)\cos\gamma. \tag{25}$$

2.6. Restrictor Flow Equation. The continuity of flow between restrictor and bearing is required to be maintained for a compensated hydrostatic/hybrid journal bearing system. Therefore, the flow through the restrictor should be taken as the boundary constraint to solve the Reynolds equation. The flow rate of the lubricant is given as follows [14, 31]:

$$\overline{Q}_R = \overline{C}_{S2}\left(1 - \overline{p}_c\right). \tag{26}$$

2.7. Boundary Conditions. The boundary conditions used for the analysis of lubricant flow field are described as follows.

(i) The nodes lying on external boundary of bearing have zero relative pressure with respect to ambient pressure, that is, $\overline{p}|_{\beta=\mp 1.0} = 0.0$.

(ii) Nodes lying on a recess have equal pressure.

(iii) Flow of lubricant through the restrictor is equal to the bearing input flow.

(iv) At the trailing edge of positive region, the Reynolds boundary condition is applied, that is, $\overline{p} = \partial\overline{p}/\partial\alpha = 0.0$.

2.8. Journal Centre Equilibrium Position. Assuming the steady state condition $\dot{X}_j = \dot{Z}_j = 0$, (21) is solved for pressure field for a specific value of journal center coordinate and the iterative procedure is continued until the equilibrium position of journal centre is achieved. For a specified vertical external radial load, the following iterative scheme is used to establish the journal centre equilibrium positions:

$$\overline{F}_x = 0; \quad \overline{F}_z - \overline{W}_o = 0. \tag{27}$$

The fluid film reaction $\overline{F}_x$ and $\overline{F}_z$ are expanded using Taylor series for ith journal centre position and correction in the journal centre displacements are obtained as [14, 31]

$$\begin{aligned}
\Delta\overline{X}^i{}_j &= -\frac{1}{D_j}\begin{bmatrix} \dfrac{\partial\overline{F}_z}{\partial\overline{Z}_j} & -\dfrac{\partial\overline{F}x}{\partial\overline{Z}_j} \end{bmatrix}\begin{Bmatrix} \overline{F_x}^i \\ \overline{F}^i_Z - \overline{W}_o \end{Bmatrix}, \\
\Delta\overline{Z}^i{}_j &= -\frac{1}{D_j}\begin{bmatrix} -\dfrac{\partial\overline{F}_z}{\partial\overline{X}_j} & \dfrac{\partial\overline{F}x}{\partial\overline{X}_j} \end{bmatrix}\begin{Bmatrix} \overline{F_x}^i \\ \overline{F}^i_Z - \overline{W}_o \end{Bmatrix},
\end{aligned} \tag{28}$$

where D_J is the determinant of the matrix $\begin{bmatrix} \dfrac{\partial\overline{F}x}{\partial\overline{X}_j} & \dfrac{\partial\overline{F}x}{\partial\overline{Z}_j} \\ \dfrac{\partial\overline{F}_z}{\partial\overline{X}_j} & \dfrac{\partial\overline{F}_z}{\partial\overline{Z}_j} \end{bmatrix}$.

The new journal center position coordinates are expressed as

$$\overline{X}_j^{(i+1)} = \overline{X}^i_j + \Delta\overline{X}^i_j, \qquad \overline{Z}_j^{(i+1)} = \overline{Z}^i_j + \Delta\overline{Z}^i_j, \tag{29}$$

where $(\overline{X}^i_j, \overline{Z}^i_j)$ are the coordinates of ith journal center position. Iterations are continued until the following convergence criterion (30) is satisfied [31, 32] as

$$\begin{aligned}
\text{PERR} &= \left[\frac{\left\{\left(\Delta\overline{X}^i{}_j\right)^2 + \left(\Delta\overline{Z}^i{}_j\right)^2\right\}^{1/2}}{\left\{\left(\overline{X}^i{}_j\right)^2 + \left(\overline{Z}^i{}_j\right)^2\right\}^{1/2}}\right] \times 100 \\
&\leq \text{TOLIM} < 0.001.
\end{aligned} \tag{30}$$

2.9. Load Carrying Capacity. Figure 2(b) depicts the distribution of load carrying capacity of a conical journal bearing.

The load carrying capacity in radial direction is expressed as follows:

$$\overline{F}_r = \overline{F}\cos\gamma = -\int_{-\lambda}^{\lambda}\int_0^{2\pi} \overline{p}\cos\gamma\, d\alpha\, d\beta. \tag{31}$$

The radial load carrying capacity is further resolved into X and Z directions as follows:

$$\begin{aligned}
\overline{F}_x &= -\int_{-\lambda}^{\lambda}\int_0^{2\pi} \overline{p}\cos\alpha\cos\gamma\, d\alpha\, d\beta \\
\overline{F}_z &= -\int_{-\lambda}^{\lambda}\int_0^{2\pi} \overline{p}\sin\alpha\cos\gamma\, d\alpha\, d\beta.
\end{aligned} \tag{32}$$

2.10. Fluid Film Stiffness and Damping Coefficients. The fluid-film stiffness coefficients are defined as the negative derivative of the load capacity with respect to the journal center displacement. Mathematically, fluid film stiffness coefficients are defined as [14]

$$\overline{S}_{ij} = -\frac{\partial\overline{F}_i}{\partial\overline{q}_j}; \quad (i = x, z), \tag{33}$$

where i: direction of force, $\overline{q}_j$: components of the journal centre displacement $(\overline{q}_j = \overline{X}_j, \overline{Z}_j)$.

The fluid film damping coefficients are defined as

$$\overline{c}_{ij} = -\frac{\partial\overline{F}_i}{\partial\dot{\overline{q}}_j}; \quad (i = x, z). \tag{34}$$

Here, $\dot{\overline{q}}_j$ represents the velocity component of journal center $\dot{\overline{q}}_j = \dot{\overline{X}}_j, \dot{\overline{Z}}_j$.

2.11. Stability Parameters. The stability of a journal bearing system is expressed in terms of threshold speed $(\overline{\omega}_{th})$, critical mass $(\overline{M_c})$. The stability parameters are defined using the Routh's stability criterion.

The nondimensional critical mass $(\overline{M_c})$ of the journal for lateral motion is expressed as

$$\overline{M}_c = \frac{\overline{G}_1}{\overline{G}_2 - \overline{G}_3}, \tag{35}$$

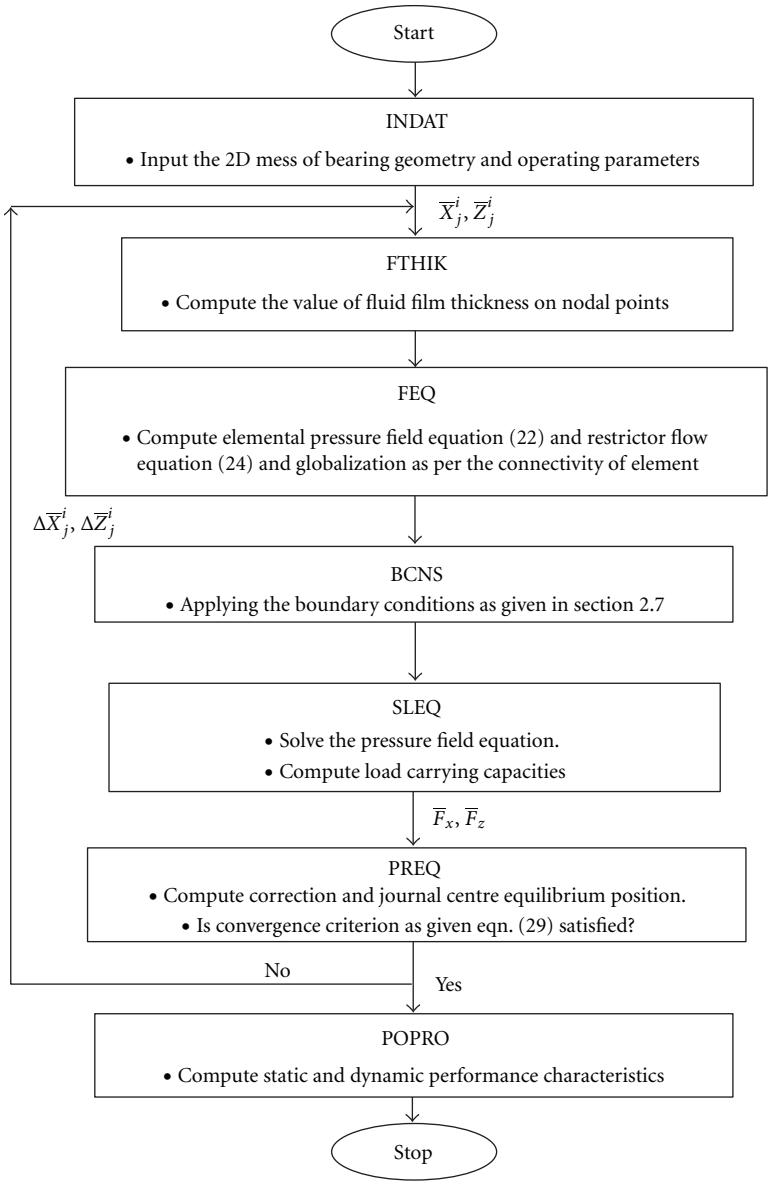

Figure 3: A flow chart to describe the overall solution scheme.

where $\overline{G}_1 = [\overline{C}_{11}\ \overline{C}_{22} - \overline{C}_{21}\overline{C}_{12}\ ]; \overline{G}_2 = [\overline{S}_{11}\overline{S}_{22} - \overline{S}_{12}\overline{S}_{21}][\overline{C}_{11} + \overline{C}_{22}]/[\overline{S}_{11}\ \overline{C}_{22} + \overline{S}_{22}\overline{C}_{11} - \overline{S}_{12}\ \overline{C}_{21} - \overline{S}_{21}\ \overline{C}_{12}\ ]; \overline{G}_3 = [\overline{S}_{11}\ \overline{C}_{11} + \overline{S}_{12}\ \overline{C}_{12} + \overline{S}_{21}\ \overline{C}_{21} + \overline{S}_{22}\ \overline{C}_{22}\ ]/[\overline{C}_{11} + \overline{C}_{12}\ ]$.

Threshold speed, that is, the speed of journal at the threshold of instability, can be obtained using the relation as follows:

$$\overline{\omega}_{th} = \left[\frac{\overline{M}_C}{\overline{F}_0}\right]^{1/2}, \tag{36}$$

where $\overline{F_0}$ is resultant fluid film force or reaction at $\partial\overline{h}/\partial\overline{t} = 0$

3. Solution Procedure

The solution for the fluid flow field of four pockets conical hybrid journal bearing system operating with both Newtonian and micropolar fluid is obtained using an iterative scheme for vertical external load as explained in Section 2.8. The pressure field equation (21) and restrictor flow equation (26) are solved together with the boundary conditions given in Section 2.7. A flow chart to describe the overall solution scheme is shown in Figure 3.

The unit INDAT reads the input data and the 2D mesh of the bearing system. Then unit FTHIK calculates the fluid film thickness at nodal points for the tentative values of the journal centre position. In unit FEQ, the fluidity matrix is generated and globalized as per the connectivity of the elements. The unit BCNS applies all the boundary conditions. In unit SLEQ, the modified Reynolds equation is solved for the fluid film nodal pressure using Gaussian elimination technique. The load carrying capacities are also computed. Utilizing the value of $\overline{F}_x$ and $\overline{F}_z$, the correction in journal centre position is computed, hence

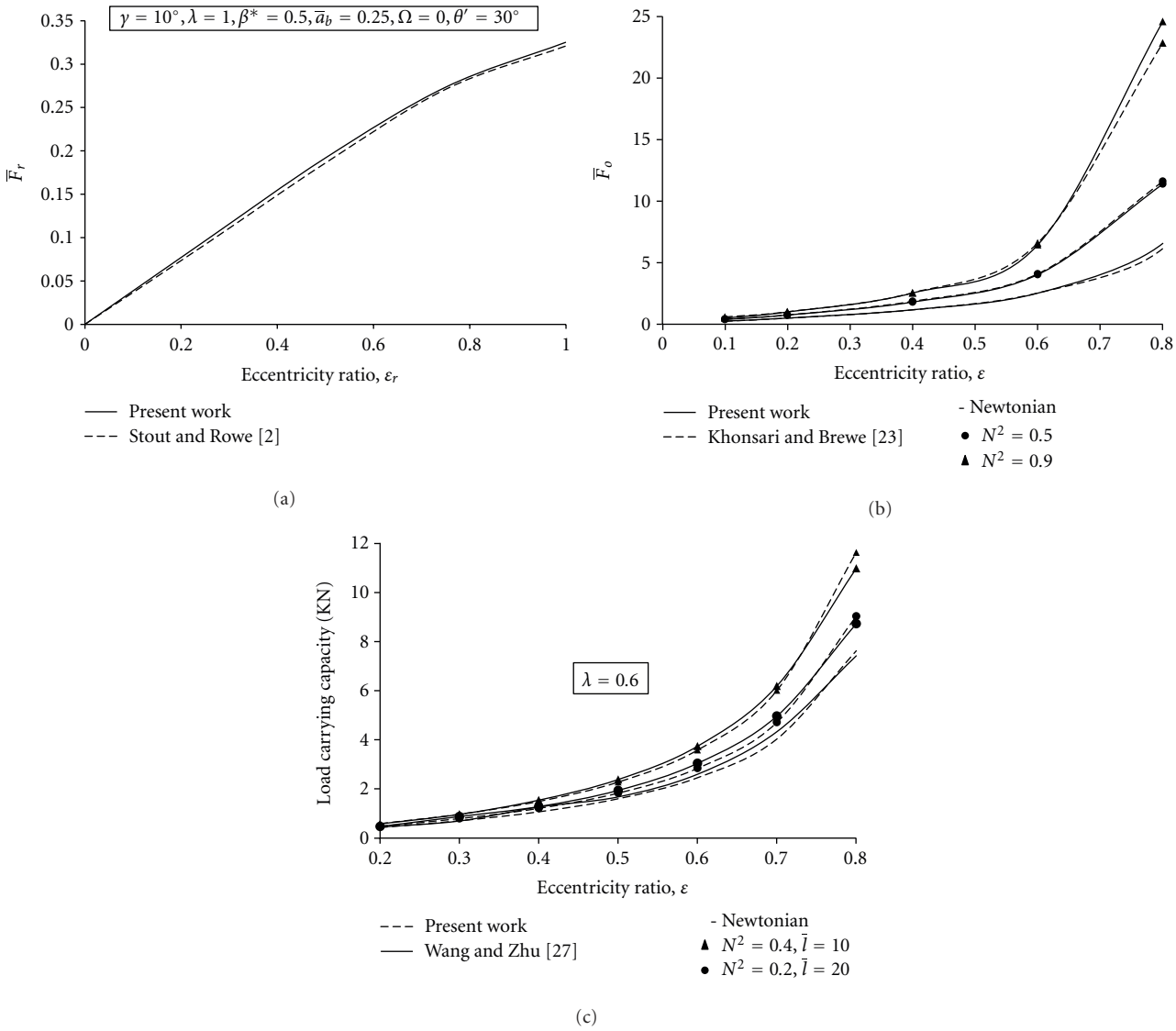

Figure 4: (a) Radial load carrying capacity ($\overline{F}_r$) versus eccentricity ratio (ε_r). (b) Load carrying capacity ($\overline{F}_o$) versus eccentricity ratio (ε). (c) Load carrying capacity (F_o) versus eccentricity ratio (ε).

the journal centre equilibrium position is computed in unit PREQ. This iterative process is continued until the convergence criterion described in (30) is satisfied. The other performance characteristics parameters are computed in unit POPRO.

4. Results and Discussion

The performance characteristics of four-pocket hybrid journal bearing system having different semicone angles for the values of micropolar parameters (coupling number and characteristic length) have been discussed. A source program has been developed in Fortran 77 using the analysis as described in earlier sections. In order to validate the methodology followed, the results of the present study have been compared with the results of Stout and Rowe [2]. Figure 4(a) depicts a favorable validation of the results of the present study with the already published results [2] with an error of 1–4%. As there are no results available for micropolar lubricated conical hydrostatic/hybrid journal bearing system, for the validation of the micropolar analysis, the results of micropolar effect in case of a circular hydrodynamic journal bearing have been compared with the already published results of Khonsari and Brewe [23] and Wang and Zhu [27]. It may be noticed from the Figures 4(b) and 4(c) the present results validate well with already published results [21, 27].

The values of bearing geometric and operating parameters chosen for conical journal bearing system are shown in Table 1. The influence of micropolar lubricant on the bearing performance characteristics has been presented with respect to the external radial load ($\overline{W}_r$) as shown through Figures 5(a)–12(a). To depict the influence of different

Table 1: Geometric and operating parameters for conical journal bearing system [2, 14, 23, 24, 29].

Bearing aspect ratio (λ)	1.0
Number of pockets	4
Restrictor design ($\overline{C}_{s2}$) parameter	0.50
Type of compensating element	Capillary
Nondimensional external radial load ($\overline{W}_r$)	0.1–0.9
Semicone angle (γ)	10°, 20°, 30° and 40°
Total pocket area to total bearing area (A_p/A_b)	0.333
Inter recess angle (θ')	30°
Speed parameter (Ω)	1.0
Land width ratio ($\bar{a}_b$)	0.25
Characteristic length ($\bar{l}$)	5, 10, 20, 30
Coupling number parameter (N^2)	0.4, 0.5

micropolar parameters on the performance of conical hybrid journal bearing, the results of performance characteristics parameters are also plotted with respect to characteristic length $\bar{l}$ for different value of coupling number at the constant value of external radial load ($\overline{W}_r = 0.5$) through Figures 5(b)–12(b).

The performance characteristics parameters of hybrid conical journal bearing for Newtonian and micropolar lubricant at the constant value of external radial load ($\overline{W}_r = 0.5$), computed in the present study are tabulated in Table 2. In the present study, performance characteristics parameters of a conical journal bearing system configuration having semicone angles 10°, 20°, 30°, and 40° have been presented for Newtonian lubricant and micropolar lubricant in the following sections.

4.1. Influence on Attitude Angle (ϕ). For a conical hybrid journal bearing system, the value of attitude angle (ϕ) increases with an increase in the value of external radial load $\overline{W}_r$ for both Newtonian and micropolar lubricant as depicted in Figure 5(a); however, the use of micropolar lubricant results in higher value of the attitude angle (ϕ) than Newtonian lubricant. Figure 5(b) depicts the variation of attitude angle (ϕ) with respect to characteristic length at the radial load ($\overline{W}_r = 0.5$) for different value of micropolar parameters. For the value of characteristic length $\bar{l} = 5$, the bearing system attains the larger value of attitude angle for each bearing configuration. Moreover, the value of attitude angle decreases rapidly up to $\bar{l} = 20$, beyond that attitude angle is almost constant. Further, it may be observed that an increase in the value of characteristic length $\bar{l}$ results in a decrease in the value of the attitude angle (ϕ). Another notable observation from Figures 5(a) and 5(b) is that higher semicone angle (γ) results in higher value of attitude angle (ϕ). The bearing configuration having semicone angle ($\gamma = 40°$) results in the higher value of attitude angle (ϕ) than other bearing configurations. Figure 5(b) also depicts that for a constant values of characteristic length, ($\bar{l}$), and radial load $\overline{W}_r$, an increase in the value of coupling number parameter (N^2) results in an increase in the value of attitude angle (ϕ).

4.2. Influence on Maximum Fluid Film Pressure ($\overline{P}_{\max}$). It may be noticed from Figure 6(a) that an increase in the value of external radial load results in an increase in the value of maximum fluid film pressure for either Newtonian or micropolar lubricant. The notable observation is that the values of $\overline{P}_{\max}$ are higher for micropolar lubricant vis-á-vis Newtonian lubricant for a specified value of radial load. Further, it may also be noticed that for bearing configurations having semicone angle ($\gamma = 10°$), the value of $\overline{P}_{\max}$ increases more rapidly with an increase in the value of radial load than other bearing configurations for either of the Newtonian and micropolar lubricants. However, for a specified radial load, the value of maximum fluid film pressure is higher for the bearing configuration having semicone angle ($\gamma = 40°$) than other bearing configurations for either of the lubricants. For bearing configuration having semicone angle ($\gamma = 10°$), at a specified value of radial load, $\overline{W}_r = 0.5$, the micropolar lubricant with characteristics $N^2 = 0.5$ and $\bar{l} = 10$ results an increase of 14.769% in the value of $\overline{P}_{\max}$ vis- á-vis Newtonian lubricant. The variation of maximum fluid film pressure with respect to characteristic length, ($\bar{l}$) of micropolar lubricant has been shown in Figure 6(b). It may be observed that for different values of coupling parameters for various configurations of semicone angle, the value of $\overline{P}_{\max}$ decreases rapidly up to the value of characteristic length $\bar{l} = 20$, beyond that the value of $\overline{P}_{\max}$ is less sensitive. It may also be noticed that for a constant values of characteristic length, ($\bar{l}$), and radial load $\overline{W}_r$, an increase in the value of coupling number parameter (N^2) results in an increase in the value of $\overline{P}_{\max}$. For the value of characteristic length, ($\bar{l} = 5$), and a coupling parameter $N^2 = 0.5$, the value of $\overline{P}_{\max}$ is higher by a factor of 21.64%, 21.023%, 19.19%, and 16.055% vis- á-vis Newtonian lubricant for semicone angles 10°, 20°, 30°, and 40° sequentially.

4.3. Influence on Minimum Fluid Film Thickness ($\overline{h}_{\min}$). It may be seen in Figure 7(a), as the value of external radial load increases, the value of minimum fluid film thickness reduces for either Newtonian or micropolar lubricant. It may be noticed that for bearing configuration having semicone angle ($\gamma = 10°$), the value of $\overline{h}_{\min}$ decreases more rapidly with an increase in the value of radial load than other bearing configurations for either of Newtonian or micropolar lubricants; however, for a specified radial load, the value of $\overline{h}_{\min}$ is lower for the bearing configuration having semicone angle ($\gamma = 40°$) than other bearing configurations for either of Newtonian or micropolar lubricants. The value of $\overline{h}_{\min}$ decreases with an increase in the value of radial load due to increase in the value of maximum fluid film pressure. For a specified value of radial load, $\overline{W}_r = 0.5$, for semicone angle $\gamma = 10°$, the value of $\overline{h}_{\min}$ of a Newtonian lubricated bearing is higher by a factor of 1.025, 1.09 and 1.209 for semicone angle 20°, 30°, and 40° sequentially. The variation of $\overline{h}_{\min}$ with respect to characteristic length, ($\bar{l}$) at a specified value of radial load, $\overline{W}_r = 0.5$, has been shown in

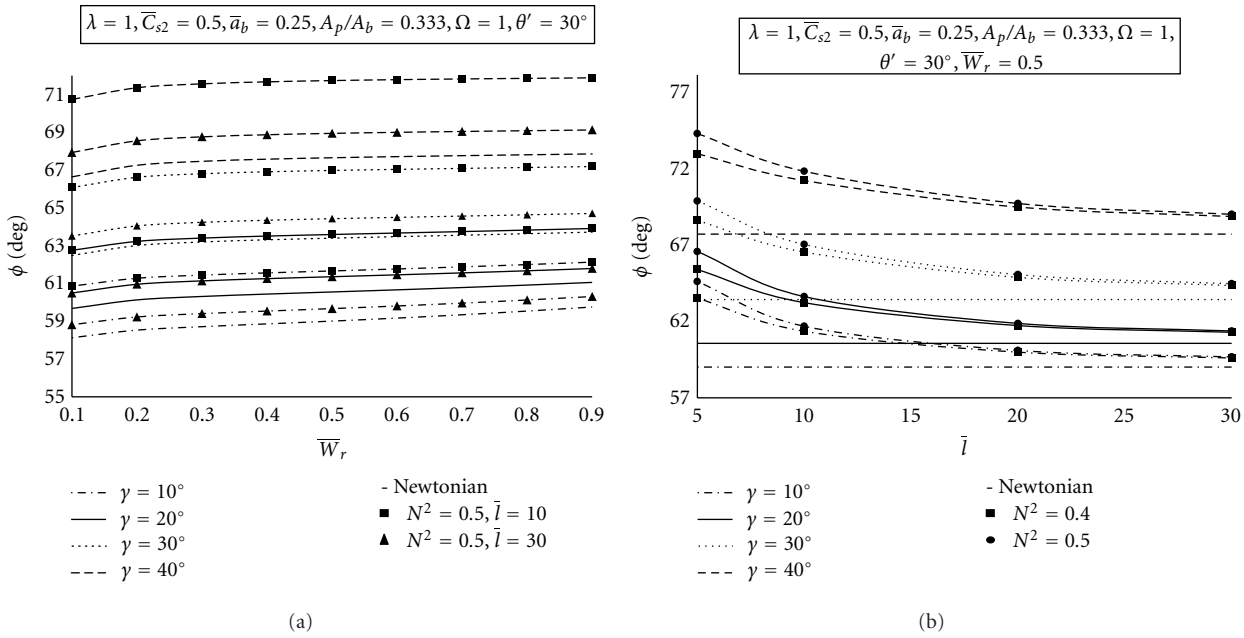

Figure 5: (a) Variation of attitude angle (ϕ) versus radial load ($\overline{W}_r$). (b) Variation of attitude angle (ϕ) versus characteristic length ($\bar{l}$).

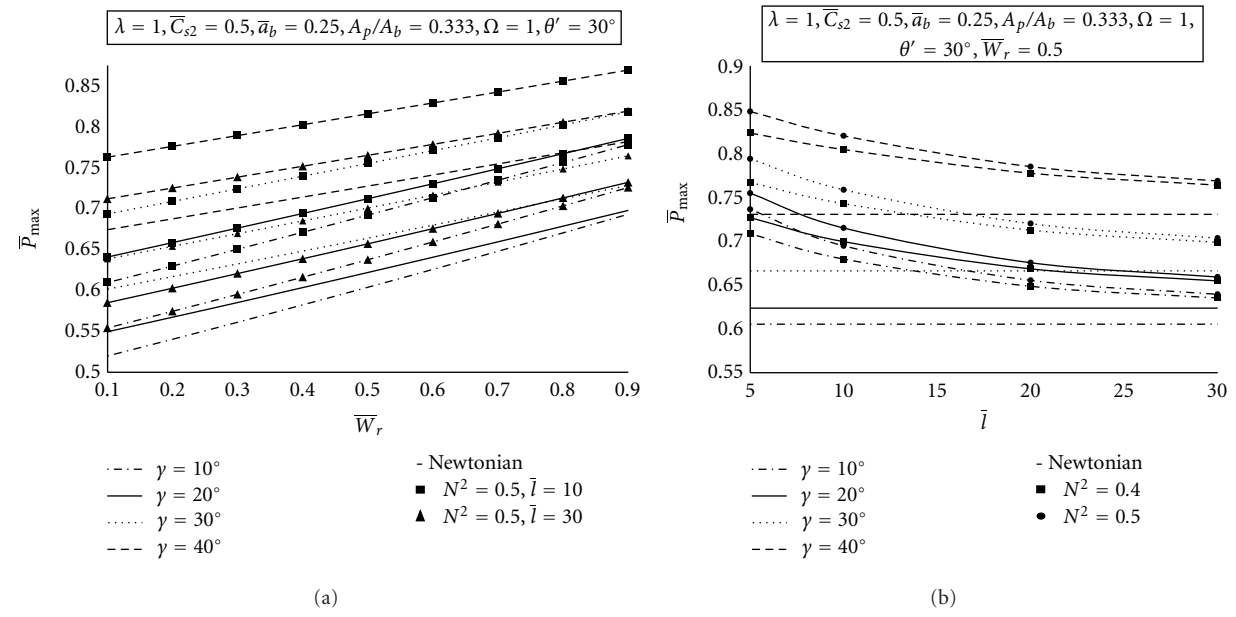

Figure 6: (a) Variation of maximum fluid film pressure ($\overline{P}_{\max}$) versus radial load ($\overline{W}_r$). (b) Variation of maximum fluid film pressure ($\overline{P}_{\max}$) versus characteristic length ($\bar{l}$).

Figure 7(b). The maximum increase in the value of $\overline{h}_{\min}$ reported at the value of characteristic length, ($\bar{l} = 5$) for different values of coupling number parameter N^2 for different semicone angle vis- á-vis Newtonian lubricant.

For the value of characteristic length, ($\bar{l} = 5$), and a coupling parameter $N^2 = 0.5$, the value of $\overline{h}_{\min}$ is enhanced by a factor of 2.94%, 2.33%, 1.77%, and 1.26% vis- á-vis Newtonian lubricant for semicone angles 10°, 20°, 30°, and 40° sequentially.

4.4. Influence on Bearing Flow ($\overline{Q}$). It may be noticed from Figure 8(a) that the value of bearing flow of a hybrid bearing system slightly increases with an increase in the value of radial load for either Newtonian or micropolar lubricants. The use of micropolar lubricant results in a decrease in the value of bearing flow than Newtonian lubricant at a specified value of load. For a specified value of radial load, the value of bearing flow is higher for bearing configuration having semicone angle ($\gamma = 10°$) than other

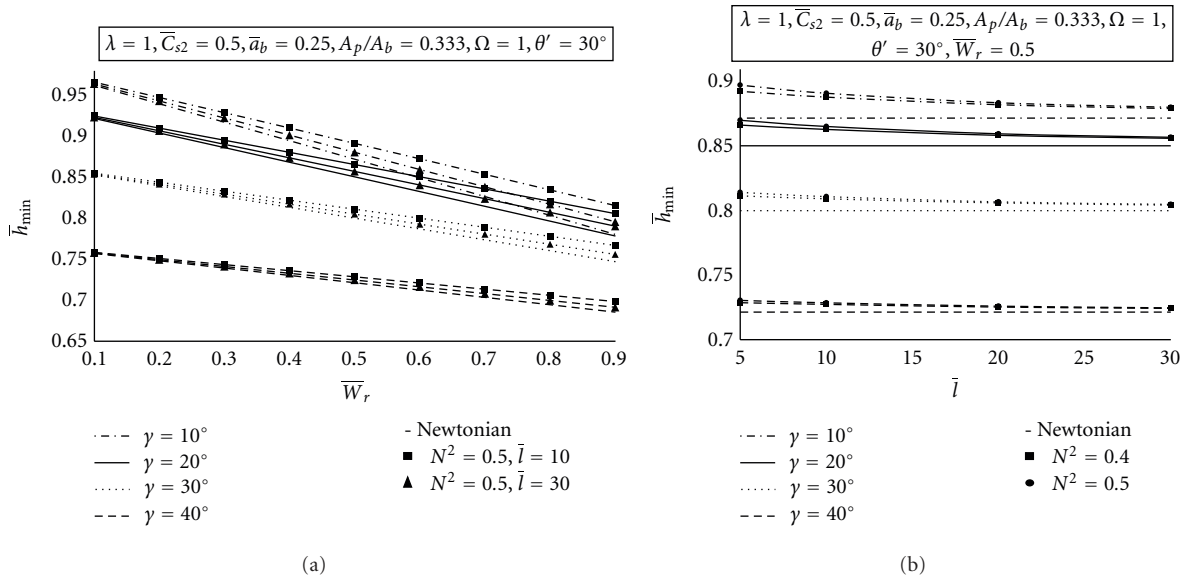

FIGURE 7: (a) Variation of minimum fluid film thickness ($\overline{h}_{\min}$) versus radial load ($\overline{W}_r$). (b) Variation of minimum fluid film thickness ($\overline{h}_{\min}$) versus characteristic length ($\overline{l}$).

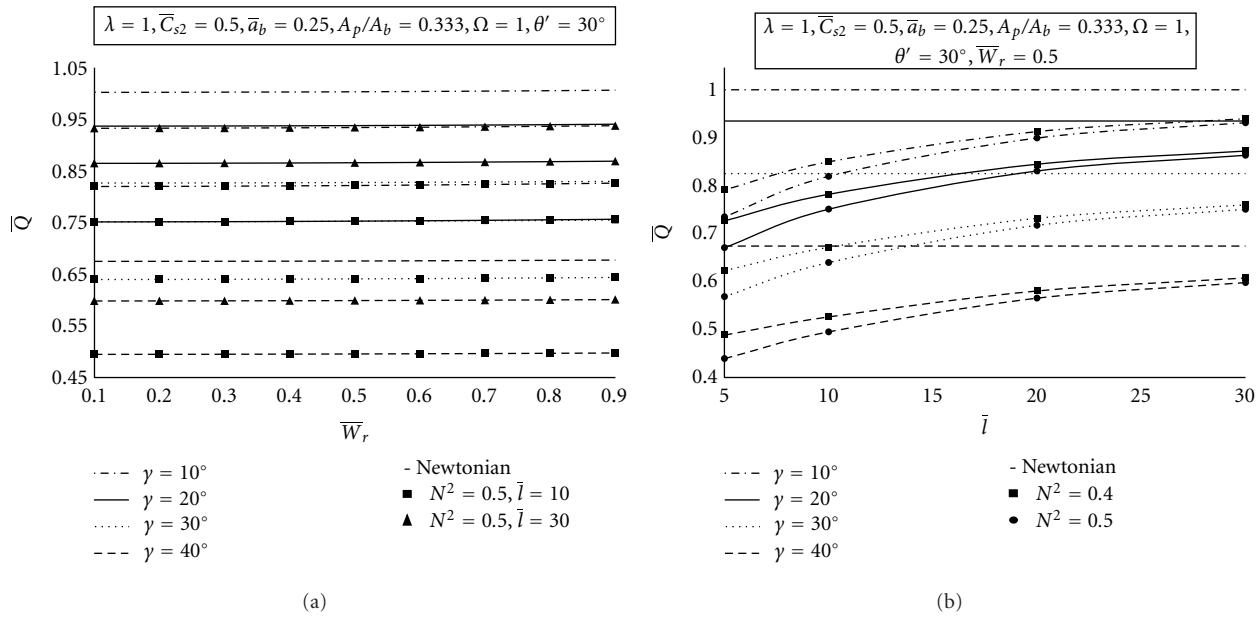

FIGURE 8: (a) Variation of $\overline{Q}$ versus radial load $\overline{W}_r$. (b) Variation of $\overline{Q}$ versus characteristic length $\overline{l}$.

bearing configurations for either the lubricants on the mode. For a specified value of radial load $\overline{W}_r = 0.5$, the use of micropolar lubricant with characteristics $N^2 = 0.5$ and $\overline{l} = 10$, the value of $\overline{Q}$ decreases by 18.10%, 19.73%, 22.50%, and 26.64% vis- á-vis Newtonian lubricant for bearing configurations having semicone angles 10°, 20°, 30° and 40° sequentially.

It may be seen from Figure 8(b) that up to the value of characteristic length, $\overline{l} = 20$, the value of $\overline{Q}$ increases rapidly for micropolar lubricant and for different values of semicone angle, beyond that the changes in the value of $\overline{Q}$ is less significant. It may also be noticed that for a constant values of characteristic length, ($\overline{l}$), and radial load $\overline{W}_r$, an increase in the value of coupling number parameter (N^2) results in a decrease in the value of $\overline{Q}$ for micropolar lubricant. Further it may be revealed that bearing system attains the lowest value of $\overline{Q}$ at the value of characteristic length, ($\overline{l} = 5$) for different semicone angles. For the value of characteristic length, ($\overline{l} = 5$), and a coupling parameter $N^2 = 0.5$, the value of $\overline{Q}$ is decreased by a factor of 26.56%, 28.32%, 31.19%, and 34.94% vis- á-vis Newtonian lubricant for semicone angles 10°, 20°, 30°, and 40° sequentially.

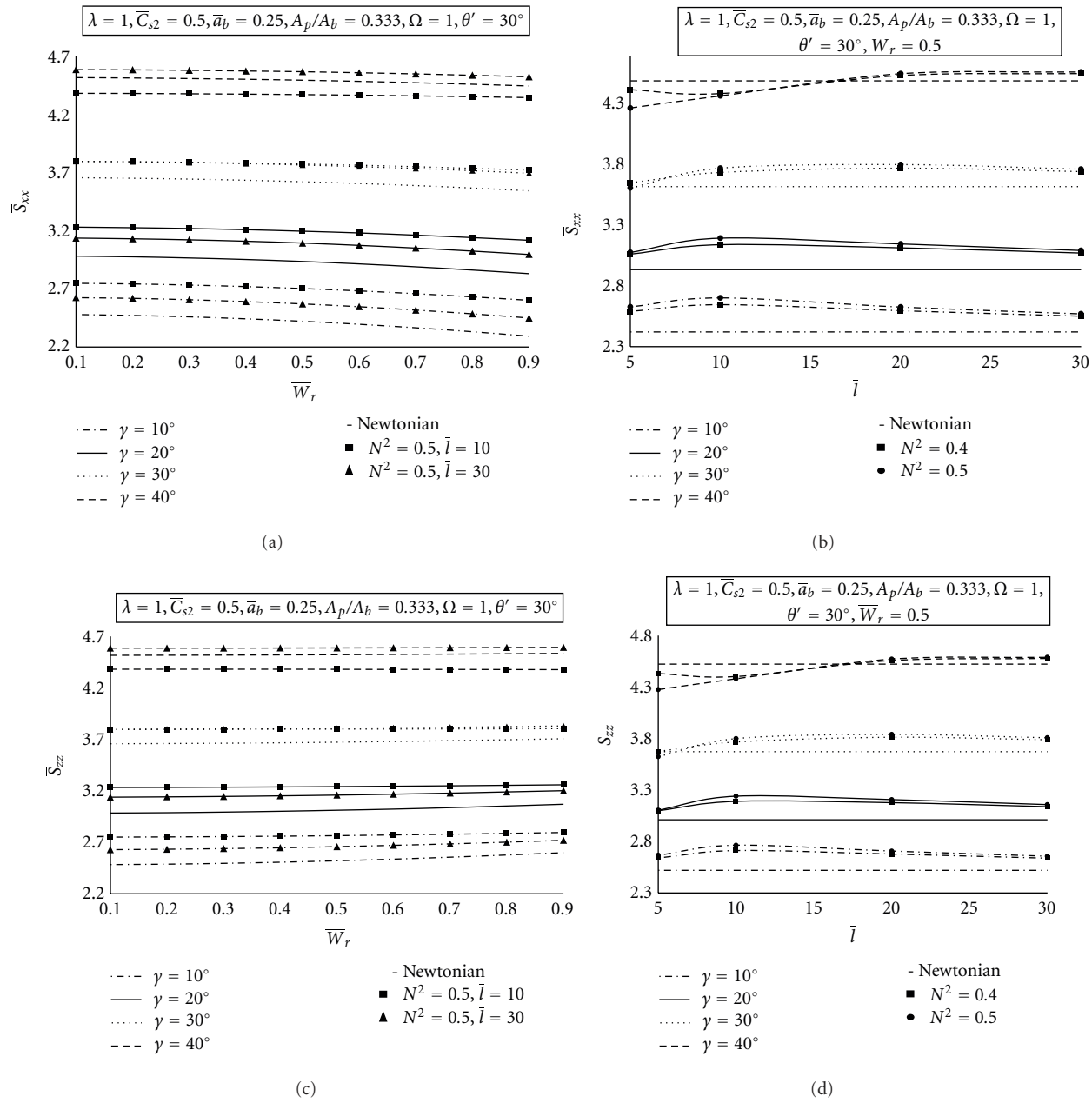

Figure 9: (a) Variation of $\overline{S}_{xx}$ versus radial load $\overline{W}_r$. (b) Variation of $\overline{S}_{xx}$ versus characteristic length $\overline{l}$. (c) Variation of $\overline{S}_{zz}$ versus radial load $\overline{W}_r$. (d) Variation of $\overline{S}_{zz}$ characteristic length $\overline{l}$.

4.5. Influence on Fluid Film Stiffness Coefficients $(\overline{S}_{xx}, \overline{S}_{zz})$. The variation in direct fluid film stiffness coefficients $(\overline{S}_{xx}, \overline{S}_{zz})$ with respect to external radial load have been shown through Figures 9(a)–9(c). Figures 9(b) and 9(d) show the variation of direct fluid film stiffness coefficients $(\overline{S}_{xx}, \overline{S}_{zz})$ with respect to characteristic length for different values of semicone angles for Newtonian and micropolar lubricated bearing system. The cross coupled stiffness coefficients $(\overline{S}_{xz}, \overline{S}_{zx})$ for a conical hybrid journal bearing system have also been computed. Their variation in this study has not been shown just for the sake of brevity. It may be clearly noticed that the variation in the values of direct fluid film stiffness coefficients $(\overline{S}_{xx}, \overline{S}_{zz})$ is not similar for all the bearing configurations studied. Up to semicone angle $\gamma = 20°$, the use of micropolar lubricant results an increase in the values of direct fluid film stiffness coefficients $(\overline{S}_{xx}, \overline{S}_{zz})$ vis- á-vis Newtonian lubricant, while for semicone angle $\gamma = 30°$ and $40°$ the use of micropolar lubricant always does not increases the values of direct fluid film stiffness coefficients $(\overline{S}_{xx}, \overline{S}_{zz})$ as shown in Figures 9(a) to 9(d). These observations indicate that the semicone angle affects the value of direct fluid film stiffness coefficients significantly. Further, it may be recalled that the micropolar function $\overline{\Phi}$ is a function of both $\overline{h}$ and $\overline{l}$, therefore, the relative magnitudes of $\overline{h}$ and $\overline{l}$

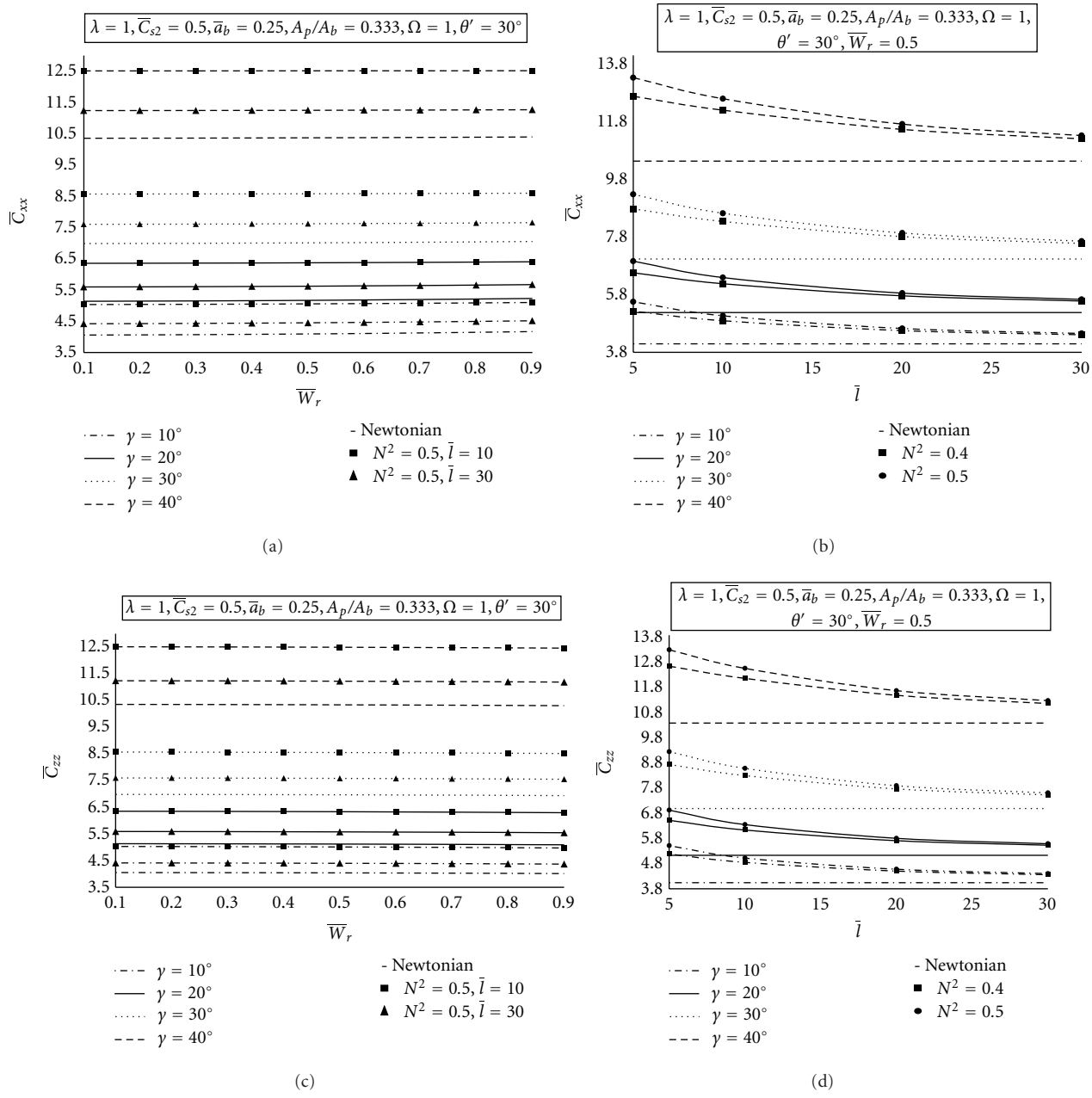

Figure 10: (a) Variation of $\overline{C}_{xx}$ versus radial load $\overline{W}_r$. (b) Variation of $\overline{C}_{xx}$ characteristic length $\overline{l}$. (c) Variation of $\overline{C}_{zz}$ versus radial load $\overline{W}_r$. (d) Variation of $\overline{C}_{xx}$ characteristic length $\overline{l}$.

affect the performance of the bearing when operated with micropolar lubricant. Further, it may be noticed that for a specified value of radial load, the values of direct fluid film stiffness coefficients $(\overline{S}_{xx}, \overline{S}_{zz})$ are higher in case of semicone angle $\gamma = 40°$ than other bearing configurations. This is due to the fact that the quantity of the lubricant is higher in case of semicone angle $\gamma = 40°$.

4.6. Influence on Fluid Film Damping Coefficients $(\overline{C}_{xx}, \overline{C}_{zz})$. It may be seen from Figure 10(a) that the value of direct fluid film damping coefficients $\overline{C}_{xx}$ increases very slightly with an increase in the value of radial load. Further it has been observed that for a specified value of radial load $\overline{W}_r = 0.5$ and for micropolar lubricant with characteristics $N^2 = 0.5$ and $\overline{l} = 10$, the value of $\overline{C}_{xx}$ increases by a factor of 23.53%, 23.26%, 22.42%, and 20.67% vis- á-vis Newtonian lubricant for bearing configurations having semicone angles 10°, 20°, 30°, and 40°. The variation of the direct fluid film damping coefficients $\overline{C}_{zz}$ with respect to load for different bearing configurations has been shown through Figure 10(c). It may be seen from Figure 10(c) that the value of $\overline{C}_{zz}$ decreases with radial load $\overline{W}_r$ for either Newtonian or micropolar lubricant. Figures 10(b) and 10(d) describes the behavior of fluid film damping coefficients $(\overline{C}_{xx}, \overline{C}_{zz})$ with respect to

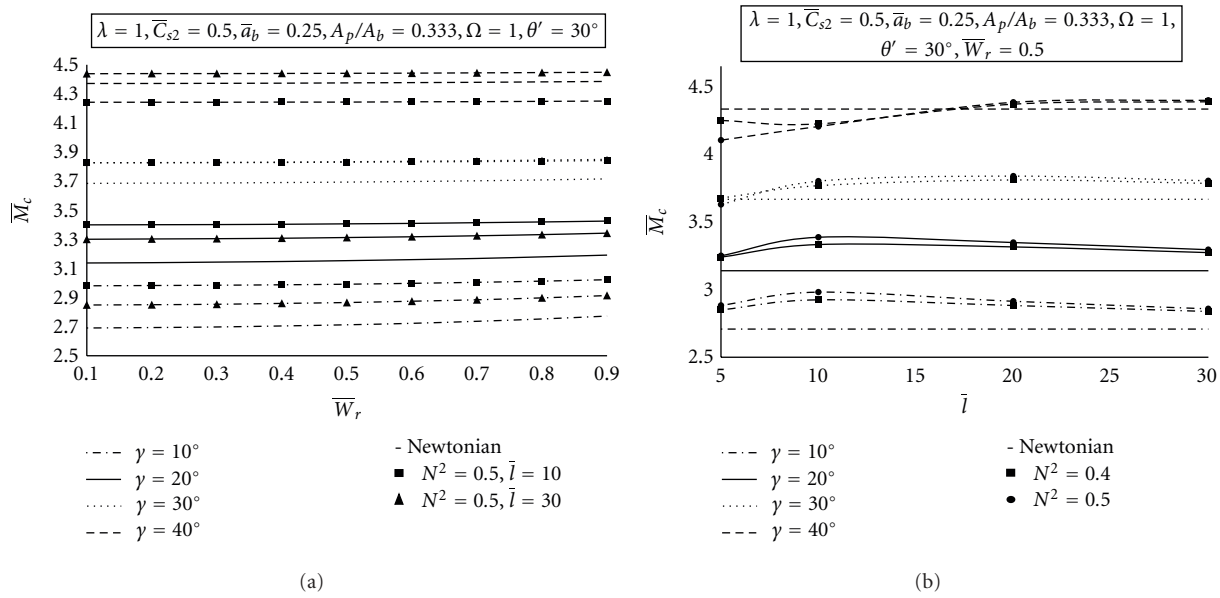

FIGURE 11: (a) Variation of $\overline{M}_c$ versus radial load $\overline{W}_r$. (b) Variation of $\overline{M}_c$ versus characteristic length $\bar{l}$.

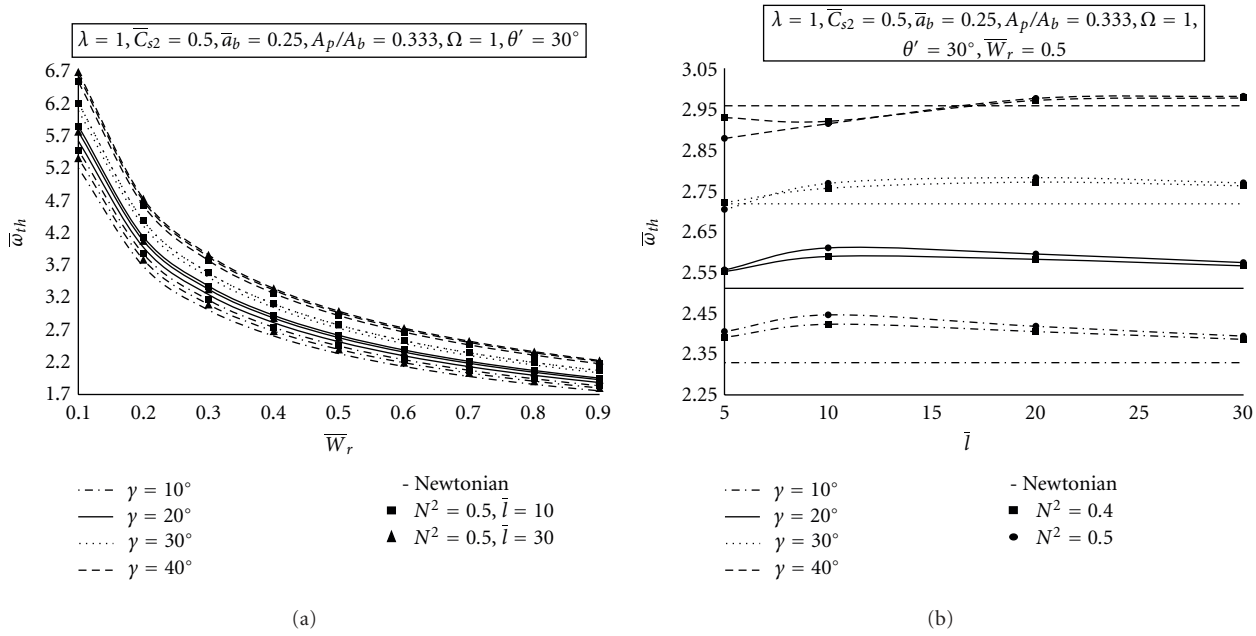

FIGURE 12: (a) Variation of $\overline{\omega}_{\text{th}}$ versus radial load $\overline{W}_r$. (b) Variation of $\overline{\omega}_{\text{th}}$ characteristic length $\bar{l}$.

characteristic length, ($\bar{l}$). From Table 2, it may be observed that for the value of characteristic length, ($\bar{l} = 5$), and a coupling parameter $N^2 = 0.5$, the value of $\overline{C}_{xx}$ gets enhanced by a factor of 35.32%, 34.17%, 31.70%, and 27.66% vis- á-vis Newtonian lubricant for semicone angles 10°, 20°, 30°, and 40° sequentially while the value of $\overline{C}_{zz}$ is raised by a factor of 36.14%, 34.79%, 32.16%, and 27.95% vis- á-vis Newtonian lubricant for semicone angles 10°, 20°, 30°, and 40° sequentially.

It may be noticed from Figures 10(a)–10(d) that for a specified value of external radial load, an increase in the micropolar effect results an increase in the value of fluid film damping coefficients ($\overline{C}_{xx}, \overline{C}_{zz}$) vis- á-vis Newtonian lubricant for each bearing configuration studied. Further, it may be noticed that for a specified value of Radial load, the value of direct damping coefficients is higher for bearing configuration having semicone angle 40^0 than other bearing configurations as depicted in Figures 10(a)–10(d). The cross coupled damping coefficients ($\overline{C}_{xz}, \overline{C}_{zx}$) for a conical hybrid journal bearing system have also been computed. Their variation in this study has not been shown just for the sake of brevity.

Table 2: Bearing performance characteristics of four-pocket conical hybrid journal bearing system operating with Newtonian and micropolar lubricant with different semicone angles.

	γ	Newtonian	$N^2 = 0.4$				$N^2 = 0.5$			
			$\bar{l} = 5$	$\bar{l} = 10$	$\bar{l} = 20$	$\bar{l} = 30$	$\bar{l} = 5$	$\bar{l} = 10$	$\bar{l} = 20$	$\bar{l} = 30$
$\overline{P}_{\max}$	10°	0.6053	0.7084	0.6796	0.6485	0.6352	0.7363	0.6947	0.6553	0.6394
	20°	0.6236	0.7268	0.6995	0.6684	0.6547	0.7547	0.715	0.6754	0.6591
	30°	0.6661	0.7669	0.7428	0.7126	0.6987	0.7939	0.7586	0.72	0.7034
	40°	0.7306	0.8233	0.8045	0.7775	0.7639	0.8479	0.8201	0.785	0.7687
$\overline{h}_{\min}$	10°	0.8721	0.8929	0.8884	0.8825	0.8795	0.8977	0.8914	0.884	0.8805
	20°	0.8506	0.8667	0.8633	0.8587	0.8564	0.8704	0.8656	0.8599	0.8572
	30°	0.8002	0.8117	0.8094	0.8062	0.8045	0.8144	0.8111	0.807	0.8051
	40°	0.7214	0.7287	0.7274	0.7253	0.7243	0.7305	0.7286	0.726	0.7247
$\overline{Q}$	10°	1.0033	0.7935	0.8522	0.9156	0.9426	0.7368	0.8218	0.902	0.9341
	20°	0.9378	0.7285	0.7841	0.8472	0.8748	0.6722	0.7528	0.833	0.8659
	30°	0.8276	0.4889	0.527	0.5814	0.6087	0.5695	0.641	0.719	0.7525
	40°	0.6756	0.4889	0.527	0.5814	0.6087	0.4395	0.4956	0.5663	0.599
$\overline{S}_{xx}$	10°	2.421	2.591	2.646	2.596	2.551	2.628	2.702	2.626	2.57
	20°	3.063	3.141	3.115	3.072	3.065	3.077	3.195	3.147	3.093
	30°	3.652	3.737	3.772	3.744	2.822	3.609	3.772	3.802	3.764
	40°	4.493	4.42	4.388	4.537	4.553	4.269	4.369	4.552	4.566
$\overline{S}_{zz}$	10°	2.52	2.64	2.712	2.678	2.638	2.667	2.764	2.707	2.657
	20°	3.011	3.099	3.19	3.177	3.138	3.104	3.24	3.207	3.158
	30°	3.672	3.674	3.766	3.812	3.788	3.624	3.799	3.84	3.807
	40°	4.522	4.43	4.402	4.557	4.577	4.275	4.38	4.571	4.588
$\overline{C}_{xx}$	10°	4.091	5.211	4.885	4.545	4.403	5.536	5.054	4.618	4.448
	20°	5.166	6.533	6.156	5.74	5.562	6.931	6.368	5.832	5.619
	30°	7.006	8.728	8.295	7.774	7.54	9.227	8.577	7.899	7.618
	40°	10.368	12.595	12.117	11.456	11.134	13.236	12.511	11.638	11.248
$\overline{C}_{zz}$	10°	4.04	5.171	4.841	4.498	4.354	5.5	5.011	4.571	4.399
	20°	5.12	6.5	6.117	5.697	5.518	6.901	6.331	5.79	5.576
	30°	6.965	8.701	8.264	7.738	7.502	9.205	8.548	7.864	7.58
	40°	10.335	12.578	12.097	11.43	11.106	13.224	12.492	11.613	11.22
$\overline{\omega}_{\text{th}}$	10°	2.329	2.391	2.423	2.405	2.386	2.405	2.446	2.418	2.394
	20°	2.511	2.552	2.589	2.582	2.566	2.556	2.61	2.595	2.574
	30°	2.718	2.721	2.756	2.771	2.762	2.704	2.768	2.782	2.769
	40°	2.958	2.929	2.92	2.971	2.977	2.878	2.914	2.976	2.981

$\lambda = 1.0$, $\Omega = 1.0$, $\overline{W}_r = 0.5$, $\overline{C}_{s2} = 0.5$, $A_p/A_b = 0.333$.

4.7. Influence on Stability Parameters ($\overline{M}_c, \overline{\omega}_{\text{th}}$). The stability is the most important issue for the fluid film journal bearing system. The stability of a bearing system is judged by critical mass of journal and threshold speed margin of the journal. Figure 11(a) shows the variation in the values of critical mass with respect to radial load for different configuration for both Newtonian and micropolar lubricant. It may be noticed that the value of $\overline{M}_c$ increases with an increase in the value of radial load. Since the critical mass of the journal is function of stiffness and damping coefficients of the bearing system, for a specified value of radial load, the use of micropolar lubricant increases the value of $\overline{M}_c$ vis-á-vis Newtonian lubricant for bearing configurations having semicone angle 10° and 20° while for bearing configurations having semicone angle 30° and 40°, the value of $\overline{M}_c$ does not always increases vis- á-vis Newtonian lubricant. The influence of coupling number on the value of $\overline{M}_c$ may be observed from Figure 11(b). The value of $\overline{M}_c$ increases with an increase in the value of coupling parameter N^2 for semicone angles 10° and 20° while in case of semicone angles 30° and 40° the value of $\overline{M}_c$ is lowered up to the value of characteristic length, ($\bar{l} = 10$), with an increase in the value of coupling parameter N^2. Further, it may also be observed that for the value of semicone angle 40° bearing system, the value of critical mass is larger than that of semicone angles 10°, 20°, and 30° for either Newtonian or micropolar lubricants.

It may be noticed from Figure 12(a) that the value of threshold speed margin decreases with radial load for each bearing configuration for both Newtonian and micropolar lubricant. However, the value of $\overline{\omega}_{\text{th}}$ decreases more rapidly up to a value of the radial load $\overline{W}_{rS} = 0.2$ for each bearing configurations. The threshold speed margin $\overline{\omega}_{\text{th}}$ is also a

function of critical mass, therefore for semicone angle 30° and 40° the different behavior of the bearing system has been reported from the view point of threshold speed margin $\overline{\omega}_{\text{th}}$. Figure 12(b) depicts the behavior of threshold speed margin for different values of coupling parameters and for different semicone angles at a specified value of radial load $\overline{W}_r = 0.5$. It may also be observed from Figures 12(a) and 12(b) that the bearing configuration having semicone angle 40^0 can sustain a higher value of threshold speed margin than the other bearing configuration for either Newtonian or micropolar lubricant.

5. Conclusion

An analytical study of a 4-pocket capillary compensated hybrid conical journal bearing system operating with micropolar lubricant has been carried out. On the basis of the numerically simulated results presented, in general, the following conclusions have been drawn.

(i) With an increase in micropolar effect of the lubricant, the value of minimum fluid film thickness $\overline{h}_{\min}$ increases. The conical bearing with semicone angle 10° provides the higher value of minimum fluid film thickness as compared to semicone angles 20°, 30°, and 40°. An increase in the value of semicone angle results in a decrease in the value of $\overline{h}_{\min}$.

(ii) The value of bearing flow $\overline{Q}$ reduces by order of 18–27% using the micropolar lubricant vis- á-vis Newtonian lubricant for different semicone angles. Bearing configuration having semicone angle 40° requires minimum bearing flow than other configuration for either Newtonian or micropolar lubricant.

(iii) The values of direct fluid film stiffness coefficients $(\overline{S}_{xx}, \overline{S}_{zz})$ increase with an increase in micropolar effect of the lubricant for semicone angles 10° and 20° while in case of semicone angle 30° and 40° decreases for higher micropolar effect of the lubricant vis- á-vis Newtonian lubricant.

(iv) The values of direct fluid film damping coefficients $(\overline{C}_{xx}, \overline{C}_{zz})$ increase with an increase in micropolar effect of the lubricant. As the semicone angle increases, the value of fluid film stiffness and damping coefficients increases.

(v) The stability in terms of critical journal mass and stability threshold speed margin increases using the micropolar lubricant for semicone angle 10° and 20°. The bearing configuration with semicone angle 40° has the larger values of stability margin than the other bearing configuration operating with both Newtonian and micropolar lubricant. The following pattern of the threshold speed margin has been observed:

$$\overline{\omega}_{\text{th}|\gamma=40^\circ} > \overline{\omega}_{\text{th}|\gamma=30^\circ} > \overline{\omega}_{\text{th}|\gamma=20^\circ} > \overline{\omega}_{\text{th}|\gamma=10^\circ}. \quad (37)$$

Abbreviations

Dimensional Parameters

a_b: Axial land width, mm
A_p: Area of the pocket, mm^2
A^e: Area of each element, mm^2
B: Body force per unit mass, N/kg
c: Radial clearance, mm
C_{ij}: Fluid film damping coefficients $(i, j = x, z)$, N/mm^2
D: Mean diameter of journal, mm
e: Journal eccentricity, mm
e_r: Journal radial eccentricity, mm
F: Fluid film reaction$(\partial h/\partial t \neq 0)$, N
F_x,F_z: Fluid film reaction components in X and Y direction $(\partial h/\partial t \neq 0)$, N
F_o: Fluid film reaction $(\partial h/\partial t = 0)$, N
h: Nominal fluid film thickness, mm
l: Characteristic length, mm
L: Bearing length, mm
L': Body couple per unit mass, $N\cdot$mm/kg
p: Pressure, N/mm^2
p_c: Pressure at recess/pocket, N/mm^2
p_s: Supply pressure, N/mm^2
Q: Lubricant flow, mm^3/sec
Q_R: Flow through restrictor, mm^3/sec
R: Radius of cone from apex, mm
r: Radius of journal at a radius R of cone
r_j: Mean Radius of journal, mm
S_{ij}: Fluid film stiffness coefficients $(i, j = x, z)$, N/mm
t: Time, sec
V: Linear velocity vector, mm/s
W_o: External load, N
x: Circumferential coordinate in Cartesian coordinate system
y: Axial coordinate in Cartesian coordinate system
X_j,Z_j: Journal center coordinate
X,Y,Z: Cartesian coordinate system
R,θ,Z: Cylindrical coordinate system
z: Coordinate along film thickness.

Greek Letters

α: Circumferential dimension of the conical journal bearing
λ: L/D, aspect ratio
θ': Inter recess angle, degree
ω_j: Journal rotational speed, rad$\cdot$sec^{-1}
ω_{th}: Threshold speed, rad$\cdot$sec^{-1}
ρ: Density, Kg$\cdot$m^{-3}
ϕ: Attitude angle, degree
Φ: Micropolar function
ϑ: Microrotation velocity vector
γ: Semicone angle, degree
λ',μ: Viscosity coefficients of the classical fluid mechanics, N-s/mm^2

χ: Spin viscosity coefficients, N-s/mm^2
$(\alpha_1, \beta_1, \gamma_1,)$: Material coefficients for a micropolar lubricant, N-s.

Nondimensional Parameters

J: Microinertia constant
$\overline{a}_b$: a_b/L
$\overline{C}_d$: Deformation coefficient
$\overline{C}_{ij}$: $C_{ij}(c^3/\mu r_j^4)$
$\overline{C}_{S2}$: Restrictor design parameter
$\overline{F}$,$\overline{F}_o$: $(F, F_o/p_s r_j^2)$
$\overline{F}_x$,$\overline{F}_z$: $(F_x, F_z/p_s r_j^2)$
$\overline{h}_{\min}$,$\overline{h}$: $(h_{\min}, h)/c$
$\overline{l}$: Nondimensional characteristic length, c/l
$\overline{M}_c$: $M_c(c^5 p_{\ s}/\mu^2 r_j^6)$
N: Coupling number, $(\chi/(2\mu+\chi))^{1/2}$
N_i,N_j: Shape function
$\overline{p}$,$\overline{p}_c$: $(p, p_c)/p_s$
$\overline{p}_{\max}$: $p_{\max}/p_s$
$\overline{Q}$: $Q(\mu/c^3 p_s)$
$\overline{S}_{ij}$: $S_{ij}(c/p_s r_j^2)$
$\overline{t}$: $t(c^2 p_s/r_j{}^2\mu)$
$\overline{W}_o$: $W_o/p_s r_j^2$
$\overline{W}_r$: $W_r/p_s r_j^2$
$(\overline{X}_j, \overline{Z}_j)$: $(X_j, Z_j)/c$
β: $R\sin\gamma/r_j$
β^*: Concentric design pressure ratio, (p^*/p_s)
ε: e/c
ε_r: e_r/c
Ω: $\omega_J(\mu r_j^2/c^2 p_s)$, speed parameter.

Matrices and Vectors

$[\overline{F}]$: Fluidity matrix
$\{\overline{p}\}$: Nodal pressure vector
$\{\overline{Q}\}$: Nodal flow vector
$\{\overline{R}_{X_j}, \overline{R}_{Z_j}\}$: Nodal RHS vectors due to journal center velocities
$\{\overline{R}_H\}$: Column vector due to hydrodynamic terms.

Subscripts and Superscripts

$-$: Nondimensional parameter
e: eth element
j: Journal
o: Steady state condition
r: Radial.

References

[1] F. M. Stansfield, *Hydrostatic Bearing for Machine Tools and Similar Application*, Machinary, London, UK, 1970.

[2] K. J. Stout and W. B. Rowe, "Externally pressurized bearings-design for manufacture Part 1-journal bearing selection," *Tribology*, vol. 7, no. 3, pp. 98–106, 1974.

[3] T. S. R. Murthy, B. R. Satyan, and R. K. Shenoy, "An analysis of a new type of high precision conical preformed four-lobe self-adjusting hydrodynamic crown bearing for grinding work spindles," *International Journal of Machine Tool Design and Research*, vol. 17, no. 4, pp. 209–224, 1977.

[4] T. J. Prabhu and N. Ganesan, "Eccentric operation of conical hydrostatic thrust bearings," *Wear*, vol. 87, no. 3, pp. 273–285, 1983.

[5] K. Srinivasan and B. S. Prabhu, "Steady state characteristics of conical hybrid bearings," *Wear*, vol. 89, no. 1, pp. 57–67, 1983.

[6] T. J. Prabhu and N. Ganesan, "Theoretical analysis of the dynamic stiffness of conical hydrostatic thrust bearings under tilt, eccentricity and rotation," *Wear*, vol. 91, no. 2, pp. 149–159, 1983.

[7] T. J. Prabhu and N. Ganesan, "Finite element application to the study of hydrostatic thrust bearings," *Wear*, vol. 97, no. 2, pp. 139–154, 1984.

[8] M. F. Khalil, S. Z. Kassab, and A. S. Ismail, "Performance of externally pressurized conical thrust bearing under laminar and turbulent flow conditions," *Wear*, vol. 166, no. 2, pp. 147–154, 1993.

[9] A. E. Yousif and S. M. Nacy, "The lubrication of conical journal bearings with bi-phase (liquid-solid) lubricants," *Wear*, vol. 172, no. 1, pp. 23–28, 1994.

[10] S. Yoshimoto, T. Kume, and T. Shitara, "Axial load capacity of water-lubricated hydrostatic conical bearings with spiral grooves for high speed spindles," *Tribology International*, vol. 31, no. 6, pp. 331–338, 1998.

[11] S. Yoshimoto, S. Oshima, S. Danbara, and T. Shitara, "Stability of water-lubricated, hydrostatic, conical bearings with spiral grooves for high-speed spindles," *Journal of Tribology*, vol. 124, no. 2, pp. 398–405, 2002.

[12] G. M. Abdel-Rahman, "The fluid flow in the thin films between the immobile conic surface," *Applied Mathematics and Computation*, vol. 153, no. 1, pp. 59–67, 2004.

[13] Q. S. LI, P. WEN, and L. X. XU, "Transition to Taylor vortex flow between rotating conical cylinders," *Journal of Hydrodynamics*, vol. 22, no. 2, pp. 241–245, 2010.

[14] S. C. Sharma, V. M. Phalle, and S. C. Jain, "Performance analysis of a multirecess capillary compensated conical hydrostatic journal bearing," *Tribology International*, vol. 44, no. 5, pp. 617–626, 2011.

[15] S. C. Sharma, V. M. Phalle, and S. C. Jain, "Influence of wear on the performance of a multirecess conical hybrid journal bearing compensated with orifice restrictor," *Tribology International*, 2011.

[16] Y. Zhang, L. Xu, and D. Li, "Numerical computation of end plate effect on Taylor vortices between rotating conical cylinders," *Communications in Nonlinear Science and Numerical Simulation*, vol. 17, no. 1, pp. 235–241, 2012.

[17] H. Hayakawa, "Slow viscous flows in micropolar fluids," *Physical Review E*, vol. 61, no. 5, pp. 5477–5492, 2000.

[18] A. C. Eringen, "Theory of anisotropic micropolar fluids," *International Journal of Engineering Science*, vol. 18, no. 1, pp. 5–17, 1980.

[19] S. J. Allen and K. A. Kline, "Lubrication theory for micropolar fluids," *Journal of Applied Mechanics*, vol. 38, no. 3, pp. 646–650, 1971.

[20] J. Prakash and P. Sinha, "Lubrication theory for Micropolar fluids and its application to a Journal Bearing," *International Journal of Engineering Science*, vol. 13, no. 3, pp. 217–232, 1975.

[21] C. Singh and P. Sinha, "The three-dimensional Reynolds equation for micropolar fluid-lubricated bearings.," *Wear*, vol. 76, no. 2, pp. 199–209, 1966.

[22] T. W. Huang, C. I. Weng, and C. K. Chen, "Analysis of finite width journal bearings with micropolar fluids," *Wear*, vol. 123, no. 1, pp. 1–12, 1988.
[23] M. M. Khonsari and D. E. Brewe, "On the performance of finite journal bearings lubricated with micropolar fluids," *Tribology Transactions*, vol. 32, no. 2, pp. 155–160, 1989.
[24] T. W. Huang and C. I. Weng, "Dynamic characteristics of finite-width journal bearings with micropolar fluids," *Wear*, vol. 141, no. 1, pp. 23–33, 1990.
[25] X. L. Wang and K. Q. Zhu, "A study of the lubricating effectiveness of micropolar fluids in a dynamically loaded journal bearing (T1516)," *Tribology International*, vol. 37, no. 6, pp. 481–490, 2004.
[26] S. Das, S. K. Guha, and A. K. Chattopadhyay, "Linear stability analysis of hydrodynamic journal bearings under micropolar lubrication," *Tribology International*, vol. 38, no. 5, pp. 500–507, 2005.
[27] X. L. Wang and K. Q. Zhu, "Numerical analysis of journal bearings lubricated with micropolar fluids including thermal and cavitating effects," *Tribology International*, vol. 39, no. 3, pp. 227–237, 2006.
[28] K. P. Nair, V. P. S. Nair, and N. H. Jayadas, "Static and dynamic analysis of elastohydrodynamic elliptical journal bearing with micropolar lubricant," *Tribology International*, vol. 40, no. 2, pp. 297–305, 2007.
[29] A. D. Rahmatabadi, M. Nekoeimehr, and R. Rashidi, "Micropolar lubricant effects on the performance of noncircular lobed bearings," *Tribology International*, vol. 43, no. 1-2, pp. 404–413, 2010.
[30] O. Pinkus and B. Sternlicht, *Theory of Hydrodynamic Lubrication*, Mcgraw-Hill, New York, NY, USA, 1961.
[31] R. Sinhasan, S. C. Sharma, and S. C. Jain, "Performance characteristics of an externally pressurized capillary-compensated flexible journal bearing," *Tribology International*, vol. 22, no. 4, pp. 283–293, 1989.
[32] J. S. Basavaraja, S. C. Sharma, and S. C. Jain, "Performance of an orifice compensated two-lobe hole-entry hybrid journal bearing," *Advances in Tribology*, vol. 2008, Article ID 871952, 10 pages, 2008.